Mechanism of destruction of the protective oxide layer on Alloy 230 in the impure helium atmosphere of Very High Temperature Reactors.

Fabien Rouillard, Céline Cabet, Stéphane Gossé, Krzysztof Wolski, Michèle Pijolat

Mechanism of destruction of the protective oxide layer on Alloy 230 in the impure helium atmosphere of Very High Temperature Reactors

Fabien Rouillard[1], Céline Cabet[1], Stéphane Gossé[2], Krzysztof Wolski[3] and Michèle Pijolat[4]

[1]*LECNA, DEN/DANS/DPC/SCCME, CEA Saclay, F-91191 Gif-sur-Yvette, France, fabien.rouillard@cea.fr, celine.cabet@cea.fr*

[2]*LM2T, DEN/DANS/DPC/SCP, CEA Saclay, F-91191 Gif-sur-Yvette, France, stephane.gosse@cea.fr*

[3]*Centre SMS/MPI, UMR-CNRS 5146, ENSM-SE, 158 cours Fauriel, F-42023 St Etienne, France, wolski@emse.fr*

[4]*Départment ProcESS, Centre SPIN, ENSM-SE, 158 cours Fauriel, F-42023 St Etienne, France, mpijolat@emse.fr*

Abstract.

Alloy 230 which contains 22wt.% chromium could be a promising candidate material for structures and heat exchangers (maximum operating temperature: 850°-950°C) in Very High Temperature Reactors (VHTR). The feasibility demonstration involves to valid its corrosion resistance in the reactor specific environment namely impure helium. The alloys surface reactivity was investigated at temperatures between 850 and 1000°C. Two main behaviours have been revealed: the formation of a protective Cr/Mn rich oxide layer at 900°C and its following destruction at higher temperatures. Actually, above a critical temperature called T_A, oxide is reduced at the oxide/metal interface by carbon in solution in the alloy. To ascribe the scale destruction, a model is proposed based on thermodynamic interfacial data for the alloy (chromium and carbon activity), oxide layer morphology and carbon monoxide partial pressure in helium. The proposed mechanism is then validated regarding experimental results and observations on alloy 230 and model alloys.

Introduction

Despite a high-level of gas-tightness and purification, cooling helium of advanced Gas-Cooled Reactors (GCR) is expected to be polluted by low levels of impurities, such as hydrogen, water vapor, methane, carbon monoxide… in the ppm to hundreds of ppm range. Structural metallic materials for pipes and heat exchangers must be resistant against corrosion at temperatures as high as 850°-950°C in this unique atmosphere which has a low oxidizing potential and a significant activity of carbon. Based on their mechanical properties and oxidation resistance, candidate alloys are nickel-based with about 20-25wt.% chromium.

Experience from former helium-cooled reactors shows that phenomena such as oxidation, carburization or decarburization may occur in impure helium depending on temperature, gas chemistry, and alloy composition. As in any other high temperature process, in GCR the corrosion resistance of chromium-rich alloys relies on the growth of a surface oxide scale that can act as a diffusion barrier. In any case, GCR environment must thus stabilize chromia. However above a critical temperature, called T_A by Brenner [1], it was observed that

chromium oxide become unstable at the alloy surface under impure helium and that carbon monoxide is released [1-6]. It is elsewhere demonstrated [7] that chromia scale is reduced by carbon from the alloy C_{sol} according to:

$$Cr_2O_3 + 3C_{sol} = 3CO(g) + 2Cr \quad (1)$$

This paper focuses on the high temperature behavior of candidate material Haynes 230® and model Ni-Cr-W-C alloys in GCR helium. It is evidenced that Eq. 1 occurs for these alloys and the critical temperature T_A is measured in various helium atmospheres. Then we characterize the system involved in the scale reduction and we develop a model based on the thermodynamic of the reaction.

Experimental set up

Materials

Haynes® alloy 230 was purchased at Haynes Int. annealed for 10 min at 1230°C then water quenched. Model alloys were manufactured with a simplified composition compared with the commercial cast: Ni22CrWC (with 22wt.% Cr — HT: 10hrs at 1350°C then 14hrs at 1100°C) and : Ni18CrWC (with 18wt.% Cr — HT: 2hrs at 1325°C then 48hrs at 1150°C). Their complete fabrication process is described elsewhere [7]. Table 1 reports the chemical composition of the alloys. For testing, 2-mm thick specimens (surface: 6 cm²) are ground to 2400 grit then finished with 1 µm alumina powder.

Table 1 Chemical composition of nickel base alloys [in wt.%]; Haynes 230®: metals by ICP-AES (CEA Saclay, DEN/DPC/SCP/LRSI); model alloys: metals by weighting; C and S by LECO® analysis (CEA Saclay, DEN/DPC/SECR/LSRM and ENSM-SE, SMS Centre)

Alloy	Ni	C	Cr	W	Mo	Fe	Mn	Al	Si	Co	Ti	Cu	La	S
Haynes 230®	base	0.105	22.0	14.7	1.3	1.3	0.5	0.4	0.4	0.2	0.1	0.02	0.005	0.002
Ni22CrWC	base	0.103	22	14								<0.001	<0.001	<0.001
Ni18CrWC	base	0.103	18	14										<0.001

Test conditions

The test procedure is fully described elsewhere [7].Generally speaking, the thermal program for the measurement of T_A consists of two steps:

step 1: heating to 900°C at 1°C/min and keeping the temperature constant for 25hrs under impure helium,

step 2: heating to 980°C (Haynes 230®) or 1050°C (model alloys) and keeping the temperature constant for 20hrs (Haynes 230®) or 3hrs (model alloys) under impure helium,

cooling: cooling at about 7.5°C/min under pure helium.

The gas flow rate is approx. 0.7ml/s per cm² of metallic surface and two heating rates were applied in step 2 (the heating was either continuous at 0.5°C/min or step-by-step with steps of 2°C and a dwell time of 30min). Table 2 gives the impurity concentrations and the water vapor partial pressure in experimental helium mixtures. In any case, oxygen, nitrogen and carbon dioxide partial pressures were below the GPC detection limit (about 0.1 µbar). As shown in Fig. 1, gas phase analysis by GPC allows to determine T_A based on the CO production: T_A is the temperature for which the increase in the CO partial pressure between the furnace inlet and outlet is equal to 1 µbar.

Table 2 Test helium composition, heating rate and measured critical temperature T_A

Helium	Alloy	CO [µbar]	H_2 [µbar]	H_2O [µbar]	CH_4 [µbar]	Heating	T_A [°C]
He-1	Haynes 230	6.1±0.1	205±4	5.0±2.4	20.0±0.4	0.5°C/min	895±5
He-2	Haynes 230	22.4±0.4	198±4	0.8±0.4	21.1±0.4	0.5°C/min	938±5
He-3	Haynes 230	21.8±0.4	200±4	0.4±0.2	19.2±0.4	2°C every 30min	940±5
He-4	Haynes 230	49.0±1.0	195±4	4.0±1.6	21.0±0.4	0.5°C/min	961±5
He-5	Haynes 230	49.0±1.0	195±4	1.6±0.8	21.0±0.4	0.5°C/min	963±5
He-6	Haynes 230	50.3±1.0	188±4	1.5±0.8	20.2±0.4	0.5°C/min	963±5
He-7	Haynes 230	52.5±1.0	196±4	0.5±0.2	21.1±0.4	0.5°C/min	969±5
He-8	Ni22CrWC	21.0±0.4	196±4	0.4±0.2	18.0±0.4	0.5°C/min	900±5
He-9	Ni22CrWC	51.4±1.0	196±4	0.8±0.4	21.1±0.4	0.5°C/min	932±5
He-10	Ni18CrWC[1]	51.2±1.0	198±4	1.1±0.6	21.1±0.4	0.5°C/min	905±5

Specimen observation and analysis

Specimens were observed either after step 1 of the test procedure or after the whole thermal program was completed (step 1 plus step 2). Surface scales were analyzed by X-Ray Diffraction (XRD with Co-Kα radiation — CEA Saclay, DEN/DPC/SCP/LRSI). Then coupons were sputtered with a gold film using cathodic evaporation and then coated by an electrolytic nickel deposit. After mounting, they were ground to 2400 grit and finished with 1 µm alumina powder. The surface was then characterized using Field Emission Scanning Electron Microscopy and Energy-Dispersive X-ray Spectroscopy (FESEM and EDS — CEA Saclay, DEN/DMN/SRMP). Thin sheets were prepared by ion sputtering and observed by Transmission Electron Microscopy (TEM and EDS — Université Paul Sabatier de Toulouse).

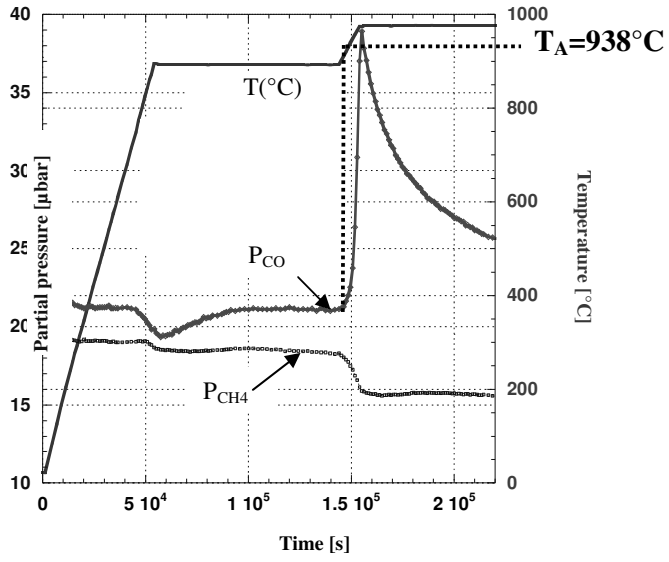

Figure 1: Thermal program and analysis of P_{CO} and P_{CH4} at the furnace outlet by GPC during testing of Haynes 230® in helium He-2

[1] The Ni-18Cr-W-C specimen did not undergo step 1 but was ex-situ pre-oxidised in Ar/1% H_2/33500 µbar H_2O at 900°C for 25 hrs ; it was rapidly heated to 850°C, then to 900°C at 0.5°C and finally followed step 2.

Results

Characterization of Haynes 230® after step 1

After step 1 of the test procedure (25 hrs at 900°C in gas mixtures of the Table 2), Haynes 230® has formed a surface scale, about 0.5-1 µm thick, as shown in the left-hand side of Fig. 2 for a treatment in helium He-5. Fig. 3 demonstrates that after exposure in atmosphere He-4 the scale is made of chromia and a mixed Cr-Mn oxide with a spinel structure. TEM observations coupled to EDS analysis, presented in Fig. 4 and Table 3, evidenced that the inner part of the scale consists of chromia (Spots ③ and ④), while manganese concentrates in the outer part (spots ① and ②).

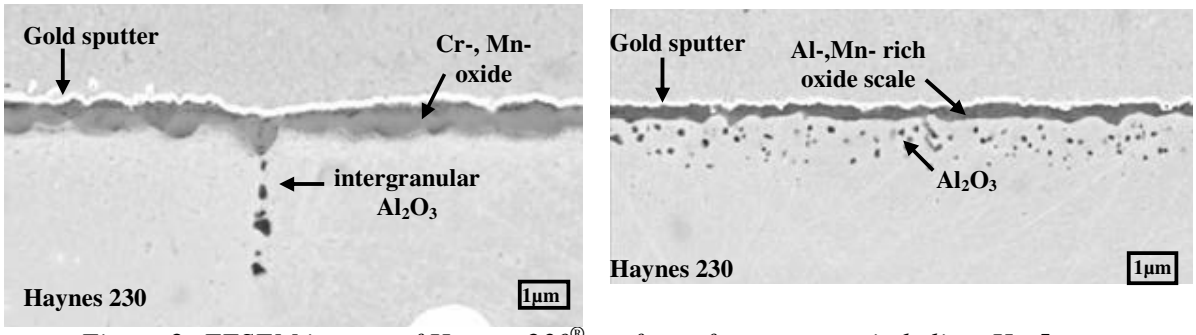

Figure 2: FESEM images of Haynes 230® surface after exposure in helium He-5; left-hand side: step 1 (25 hrs at 900°C) and right-hand side: step 1 + step 2 (20 hrs at 980°C)

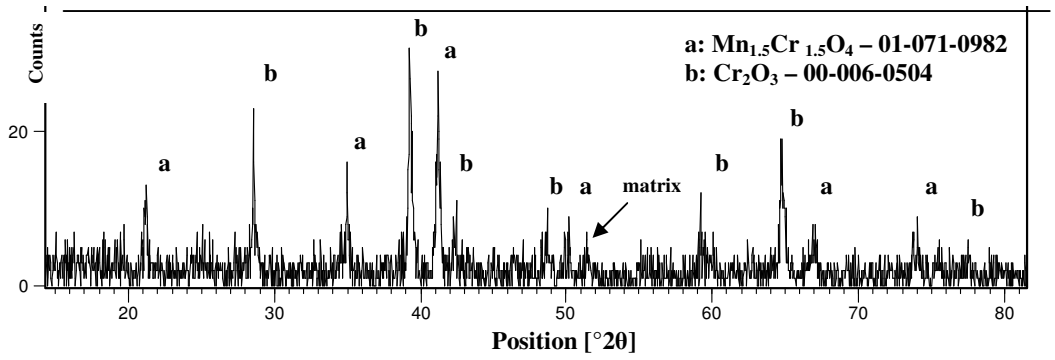

Figure 3: Low angle XRD analysis (1°) of Haynes 230® surface after step 1 in helium He-4

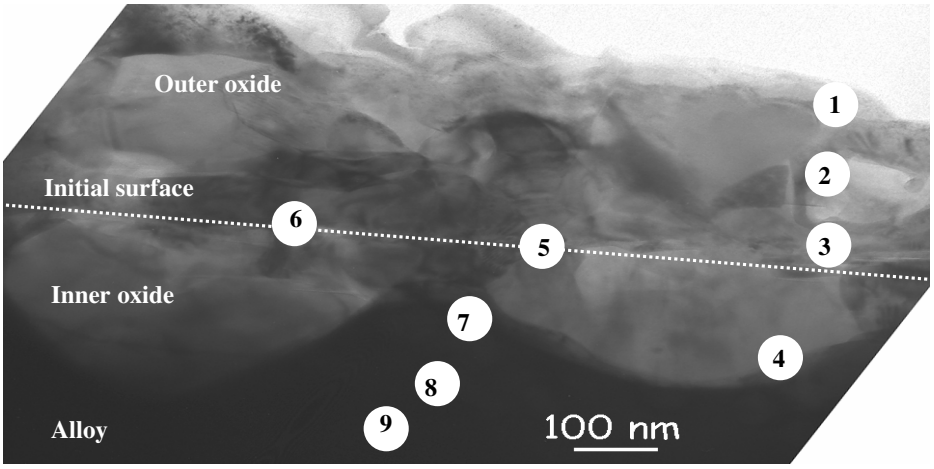

Figure 4: TEM image of Haynes 230® surface scale after step 1 in helium He-4
Numbers refer to the EDS analyses shown in Tables 3 and 4

In Fig. 4, the initial alloy surface is marked by small alumina nodules which develop in the very early stages of oxidation (spots ⑤ and ⑥ with their composition given in Table 3). Aluminum is also detected in the internal oxide either as alumina or dissolved in chromia (spot ④).
Fig. 4 and Table 4 also show that, underneath the oxide/metal interface, the substrate has been depleted in chromium due to Cr-rich oxide growth. This depletion is significant (15wt.% at spot ⑦ for an initial concentration of 22wt.%), but steep: at a depth of 500nm the alloy recovers its bulk chromium content. This marked Cr profile is in agreement with the observations made by Tawancy et al. [8] on Haynes 230® oxidized in air and could be due to the high content of tungsten, element that is known to lower the diffusion rates within the matrix [9]; therefore the transport of Cr from the bulk to the surface may be slowed down.

Table 3: EDS analyses in the oxide scale — Numbers refer to the EDS spots in Fig. 4

Spot	Cr [at.%]	Al [at.%]	Si [at.%]	Ni [at.%]	Mn [at.%]	O [at.%]
①	29			2.5	10.6	57
②	28			4.0	10.0	57
③	34			3.0		63
④	31	4.8		1.6		62
⑤	40	10.3	0.6	2.0		47
⑥	18.2	17.3	3.7	1.6		59

Table 4: EDS analyses in the metal — Numbers refer to the EDS spots presented in Fig. 4

Spot	Cr [wt.%]	W [wt.%]	Ni [wt.%]	Mo [wt.%]
⑦	15	14	68	1.8
⑧	16	14	68	1.0
⑨	18	12	68	1.6

Characterization of Haynes 230® after step 2

Cr-rich surface oxide is destroyed during step 2 of the thermal program (heating up to 980°C and maintain for 20 hrs) with a carbon monoxide release (see Fig. 1). The extent of the scale removal depends on gas composition in helium. Fig. 4 evidences that the ~1 µm-thick Cr/Mn-oxide scale, grown after step 1 in atmosphere He-5 (left-hand side), is partly reduced during step 2 (right-hand side). Inclusions of aluminum oxide remain, as Al can not react in the given temperature range [6].

Characterization of model alloys

After step 1 of the test procedure (25 hrs at 900°C) in atmospheres He-8 to He-10, model alloys have developed a scale made of pure chromia as other elements (Ni, W) are not able to react in the given conditions. During step 2, this scale is reduced in impure helium and a production of carbon monoxide is observed (see ref. [7]).

Determination of the critical temperature T_A

Following the test procedure previously described, T_A is measured for Haynes 230® and model alloys under various helium atmospheres. The results are reported in Table 2.

Discussion

Reaction mechanism

During heating at the beginning of step 2, the surface scale is reduced by carbon from the alloy following Eq. 1 (see demonstration in ref. [7]). As carbon is not soluble in chromium-oxide [10], the reaction inevitably occurs at the oxide/metal interface where carbon can be in contact with the oxide. Fig. 4 shows that in Haynes 230® the interfacial oxide is made of chromia with some alumina. Model alloys, whose only oxide-former element is Cr, quite obviously form chromia scale. So at the very first step of the reaction, reduction of the scale occurs at the oxide/metal interface and affects the following system: chromia (possibly doped in Al in the case of Haynes 230®) plus carbon in solution in the alloy according to:

$$Cr_2O_3 + 3C^i_{sol} = 3CO^i(g) + 2Cr^{bcc} \quad (2)$$

where the suffix i refers to the oxide/metal interface and Cr^{bcc} is pure chromium.
The observation of carbon monoxide production starting at T_A requires that two main steps take place: the reaction between chromia and carbon at the oxide/metal interface (Eq. 2) to give CO and pure chromium - with then a dissolution of chromium in the alloy since no pure chromium area could have been evidenced - and the transport of the produced carbon monoxide through the scale from the interfacial reaction site to the gas phase. Thus at T_A, Eq. 2 is on the right hand side and $P(CO^i) \geq P(CO^{gas})$. Table 2 (He-2 and He-3) shows that the rate of heating in step 2 does not influence the value of T_A. This implies that the transport of CO through the scale is fast compared to reaction Eq. 2. This transport is so high (see Fig. 1) that it shall occur via gas diffusion. Because no microcracks have been evidenced by FESEM into the oxide layer, the high diffusion paths are probably of nanometric size, some authors talk about nanochannels. A lot of mechanisms for the formation of nanochannels in oxides have been proposed [11,12,13] but what is most likely in this case is the presence of insoluble phases such as carbides or aluminum rich oxides that early segregate on the original surface and prevent the Cr-rich oxide layer from growing perfectly gas-tight [13]. Thus the

nanochannel network should already exist at the oxidation step (step 1) although it would have a negligible role in the overall oxide development mainly driven by outward growth.
As a consequence of this high diffusion of CO through the oxide layer, we will consider that $P(CO^i)=P(CO^{gas})$. This observation is in agreement with the proposition made by Quadakkers [2] who stated that T_A is the equilibrium temperature of the chromia reduction by carbon (Eq. (1)). Assuming that T_A is the equilibrium temperature of Eq. 2, the reaction constant can be then written as:

$$K_2(T_A) = \frac{a_{Cr^{bcc}}{}^2}{a_{Cr_2O_3}.a_{C^i_{sol}}{}^3}.\left(P(CO^i)\right)^3 = \frac{P(CO^{gas})^3}{a_{C^i_{sol}}{}^3} \quad (3)$$

with the activities of pure phases Cr_2O_3 and Cr^{bcc} taken as unity.

Determination of the activity of carbon at the oxide/metal interface $a(C_{sol}^i)$

At high temperature, the activity of carbon in multiphase alloys depends on the carbide nature as well as on the chemical composition, especially the content in carbide-former elements. ThermoCalc® [14] is used to calculate $a(C_{sol}^i)$ at T_A. This thermodynamics software minimizes the free energy of a complex system (CALPHAD® method). Two relevant databases are available for nickel-base alloys under the brand names: SSOL2 [15] and TTNi7. For the Haynes 230® chemical composition (see Table 1) in the temperature range 850°-1000°C, TTNi7 predicts the precipitation of M_6C-type carbides whereas SSOL2 proposes carbides of the $M_{23}C_6$ type.

Carbides within as-received and aged specimens of Haynes 230® were characterized by TEM; heat treatment were performed at 850°, 900° and 950°C for 25, 1000 or 5000 hrs:

- The as-received alloy contains large intragranular carbides. EDS analyses, given in Table 5, is in good agreement with the results of Grimmer $(Ni_{1.9}Fe_{0.1}Cr_{1.6}Si_{0.2})(W_{1.6}Mo_{0.6})C$ [16]. Because of their size, it is not possible to obtain diffraction images but the composition corresponds to the stoichiometry M_6C with a likely structure of the Ni_3W_3C type [17]. Besides few small Cr-rich carbides of the $M_{23}C_6$ type are evidenced at grain boundaries (see Table 5).
- Ageing for 25 hrs induces a significant formation of Cr-rich $M_{23}C_6$ carbides within grains, at grain boundaries and around primary M_6C carbides (see Table 5). Fig. 5 shows the development of $M_{23}C_6$ carbides next to a primary M_6C after 25 hrs at 900°C. Growth of $M_{23}C_6$ carbides in the vicinity of the M_6C might result from a partial dissolution of the M_6C at the expense of $M_{23}C_6$ [18]. The precipitation of $M_{23}C_6$ is observed at any temperature and enhances with the ageing time.

Thus $M_{23}C_6$ seem to be the more stable carbides in Haynes 230® above 850°C.
XRD analysis of as-received model alloys shows that the only carbides present are $M_{23}C_6$. These carbides are maintained after ageing for 25 hrs at 900°C.

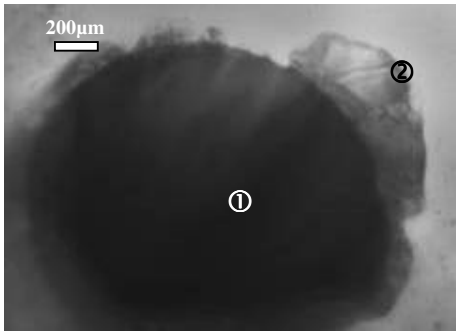

Figure 5: TEM image of Haynes 230® aged for 25 hrs at 900°C - $M_{23}C_6$ (②) carbide next to a primary carbide M_6C (①)

Table 5: Chemical composition of carbides [at.%] in Haynes 230®

specimens	carbide	Ni	Cr	W	Mo	Fe
as-received	M_6C	36	27	30	6	1
as-received	$M_{23}C_6$	14	74	8	4	/
aged for 25 hrs	① in Fig. 5	35	27	30	6	1
aged for 25 hrs	② in Fig. 5 ($M_{23}C_6$)	12	76	8	4	/

SSOL2 database was selected for further work since it gives a better description of the phases present in the system at 850°-1000°C with stable $M_{23}C_6$ carbides. The activity of carbon at the oxide/metal interface $a(C_{sol}^i)$ is then estimated by inputting the interfacial chemical composition of the alloy in the software with SSOL2 database. It is noteworthy that ThermoCalc® basically calculates the carbon activity (with graphite as the reference phase at all temperatures) by the equilibrium:

$$M_{23}C_6 = 23M^i + 6C_{sol}^i \quad (4)$$

with M= 86at.% Cr, 8at.% W, 6at.% Ni.
Considering the high chromium content in the $M_{23}C_6$ carbides, the chromium activity plays a key role in Eq. 4 and consequently on $a(C_{sol}^i)$. Therefore, the chromium activity at the oxide/metal interface $a(Cr^i)$ must be accurately known.

Determination of the chromium activity at the oxide/metal interface a(Cri)

The chromium activity is determined at the oxide/metal interface via the formula:

$$a_{Cr^i}(T) = \gamma(T).\%Cr^i \quad (5)$$

with $\%Cr^i$ the interfacial weight percentage of chromium (at any temperature, the reference state is the pure bcc Cr). $\%Cr^i$ was measured by TEM-EDS as shown in Fig. 4 and Table 3. $\gamma(T)$ is extrapolated in the range 850-1000°C from data published in ref. [19] for higher temperatures. For a given alloy, it is assumed that $\gamma(T)$ is independent of %Cr.

Assessment of the model

Fig. 6 summarizes the steps used in the model that allows to evaluate the relationship between P(CO) and T_A: $\%Cr^i$ is analyzed at the oxide/metal interface using the EDS detector in a TEM, $a(Cr^i)$ is deduced via Eq. 5 with γ respect to ref. [19, 20], then $a(C_{sol}^i)$ is computed using ThermoCalc® software with the SSOL2 database. Finally, Eq. 3 correlates P(CO) and $1/T_A$ by taking $K_2(T)$ from ref. [21].

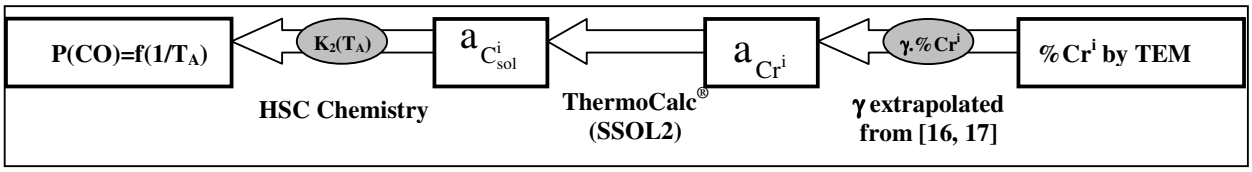

Figure 6: Model developed to correlate theoretical T_A to experimental T_A

Table 6 gives, for the three alloys, the interfacial concentrations of chromium analyzed by TEM-EDS after step 1 of the test procedure (25 hrs at 900°C). The method depicted in Fig. 6 was applied. Taking into account the experimental uncertainties on $\%Cr^i$ (by TEM/EDS) as well as on γ (by Knudsen cells [19]), one obtain minimum and maximum values for $a(C_{sol}^i)$. Table 7 develops the calculations for Haynes 230®.

Table 6: Experimental $\%Cr^i$ by TEM-EDS analysis after step 1 of the test procedure

	Haynes 230®	**Ni22CrWC**	**Ni18CrWC**
$\%Cr^i$ [wt.%]	15-16	15-16	13-14

Table 7: Lower and upper theoretical values of log[P(CO)] at different temperatures calculated by the model shown on Fig. 6 considering the data of Tables 6 and 7

		$(\%Cr^i)^{min}$ = 15 wt.%			**$(\%Cr^i)^{max}$ = 16 wt.%**		
T[°C]	**γ(T)**	**$a(Cr^i)^{min}$**	**$a(C_{sol}^i)^{min}$**	**$Log(P_{CO})^{min}$**	**$a(Cr^i)^{max}$**	**$a(C_{sol}^i)^{max}$**	**$Log(P_{CO})^{max}$**
900	3.73±0.22	0.53	$4.8.10^{-3}$	-5.08	0.63	$2.4.10^{-3}$	-5.39
950	3.21±0.19	0.45	$1.1.10^{-2}$	-4.23	0.54	$5.6.10^{-3}$	-4.54
1000	2.79±0.17	0.39	$2.5.10^{-2}$	-3.44	0.47	$1.3.10^{-3}$	-3.75

Fig. 7 reports the results on T_A from Table 2 and plots the theoretical lines log(P(CO)) vs. $1/T_A$ for the commercial Haynes 230® (see Table 7) and two model alloys. Because of the uncertainties on $a(C_{sol}^i)$, the model gives a scatter band delimited by a lower curve corresponding to the minimum $a(C_{sol}^i)$ and an upper curve for the maximum $a(C_{sol}^i)$. For all three alloys, the experimental critical temperatures T_A exactly fall within the theoretical scatter band. This excellent fit in the whole temperature range, is a further hint that the transport of CO through the oxide scale does not affect the kinetic of reaction (2).

It is however worth noticing that the slope of the experimental curves seems to be slightly less than predicted by the theory. On the one hand, one should recall that an experimental T_A is not exactly the equilibrium temperature of Eq. 2, but actually the temperature for which the CO production reaches 1µbar (see section 'Experimental'). This could be a reason why the measured T_A globally fall in the upper part of the scatter band. On the other hand, the activity coefficients were measured in the range 1150°-1300°C then extrapolated to intermediate temperatures (850°-1000°C). The chromium activity at the lowest temperatures (850°-900°C) may thus be overestimated. As a consequence, the theoretical curves would bend a little

towards the higher log[P(CO)] values at the lower temperatures as is observed for the experimental results.

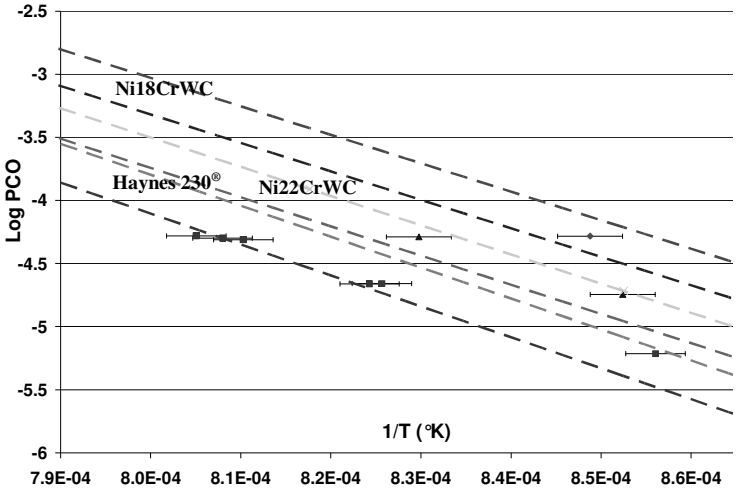

Figure 7: Log(P(CO))=f(1/T_A) for Haynes 230® and model alloys – experimental data and theory

Conclusion

A model is developed to rationalize the variation of the critical temperature for surface oxide removal T_A as a function of the CO partial pressure in the gas phase. It was proposed that at the early stages of the scale reduction the relevant thermodynamic system is: chromia plus carbon in solution in the alloy at the oxide/metal interface. The interfacial activity of carbon in the alloy is calculated based on measurements of the interfacial weight percentage of chromium in equilibrium with Cr rich $M_{23}C_6$ carbides and using the ThermoCalc® software. Excellent agreement is observed between experimental values T_A and the theoretical predictions.

References

[1] K.G.E. Brenner, L.W. Graham, Nucl. Technol., 66 n°2 (1984), p. 404-414
[2] W. J. Quadakkers, H. Schuster, Werkstoffe und Korrosion 36 (1985), p. 141-150 & p. 335-347
[3] M. R. Warren, High Temp. Technol. 4 (1986), p. 119-130
[4] J. Christ, U. Künecke, K. Meyer, H. G. Sockel, Mater. Sci. Eng. A 87 (1987), p. 161-168
[5] J. Chapovaloff, D. Kaczorowski, K. Wolski, Proc. Matériaux 2006, Dijon, France (2006)
[6] F. Rouillard, C. Cabet, K. Wolski, M. Pijolat, Ox. Met. 68 (2007), p. 133-248
[7] C. Cabet, G. Girardin, F. Rouillard, J. Chapovaloff, K. Wolski, M. Pijolat, Mat. Sci. For. 595-598 (2008), p. 439-448
[8] H. M. Tawancy, Ox. Met. 45 n°3/4 (1996), p. 323-348
[9] M. Levy, P. Farell and F. S. Petit, Corr. NACE, 42 (1986), p. 708
[10] I. Wolf, H. J. Grabke, P. Schmidt, Ox. Met. 29 n°3/4 (1988), p. 289-306
[11] G. B. Gibbs, Ox. Met. 7 n°3 (1973), p. 173-200
[12] P. Kofstad, Ox. Met. 44 n°1/2 (1995), p. 3-25
[13] I. Wolf, H. J. Grabke and P. Schmidt, Ox. Met. 29 n°3/4 (1988), p. 289-306

[14] Thermo-Calc version Q: Foundation for Computational Thermodynamics, Stockholm, Sweden, Copyright (1993, 2000) SGTE, Scientific Group
[15] Thermodata Europe Database version 2
[16] H. Grimmer, EIR Report n°555, Swiss Federal Institute for Reactor Research (1985), p. 55-62
[17] H. M. Tawancy, J. Mater. Sci. 27 (1992), p. 6481
[18] E. Ross and W. Sims, Superalloys II John Wiley & Sons, Sims, Stoloff and Hagel Eds. (1987), p. 111
[19] S. Gossé, T. Alpettaz, F. Rouillard, S. Chatain, C. Guéneau, C. Cabet, Mat. Sci. For. 595-598 (2008), p. 975-985
[20] F. Rouillard, PhD thesis, Ecole Nationales Supérieures des Mines de Saint Etienne (2007)
[21] HSC Chemistry 5.11, Outokompu Research Oy, Pori, Finland (2002)